

NOVEL TWO DIMENSIONAL CYANIDE-BRIDGED METAL NANOSHEETS:
CRYSTALLOGRAPHIC STUDY AND PREPARATION
BY EXFOLIATION

THESIS

Presented to the Graduate Council of
Texas State University-San Marcos
in Partial Fulfillment
of the Requirements

for the Degree

Master of SCIENCE

by

Tyler Lee Nash, B.S.

San Marcos, Texas
December 2011

NOVEL TWO DIMENSIONAL CYANIDE-BRIDGED METAL NANOSHEETS:
CRYSTALLOGRAPHIC STUDY AND PREPARATION
BY EXFOLIATION

Committee Members Approved:

Gary W. Beall, Chair

Clois E. Powell

Benjamin R. Martin

Approved:

J. Michael Willoughby

COPYRIGHT

by

Tyler Lee Nash

2011

FAIR USE AND AUTHOR'S PERMISSION STATEMENT

Fair Use

This work is protected by the Copyright Laws of the United States (Public Law 94-553, section 107). Consistent with fair use as defined in the Copyright Laws, brief quotations from this material are allowed with proper acknowledgment. Use of this material for financial gain without the author's express written permission is not allowed.

Duplication Permission

As the copyright holder of this work I, Tyler Lee Nash, authorize duplication of this work, in whole or in part, for educational or scholarly purposes only.

ACKNOWLEDGEMENTS

I would like to thank Dr. Beall for his guidance and knowledge imparted throughout my research and the composition of this thesis. His influence on my educational knowledge and experience will no doubt be carried throughout my professional and academic career. I would also like to thank Dr. Martin and Dr. Powell for taking the time to teach me many of the skills I have acquired throughout my education and for providing valuable feedback when I needed it the most. I would also like to thank all of the members of Dr. Beall's research group for their support and camaraderie. I would like to acknowledge the aid provided by the Department of Physics, especially the training and support provided by Eric Schires.

Most of all I would like to thank my wife, Yelena, for her patience and understanding throughout the pursuance of my education. Had it not been for her loving and loyal companionship I would surely not have achieved the level of success that is now possible. Her knowledge of chemistry has aided me throughout my educational career and in my research. I would also like to thank my parents for supporting me throughout my education. I would not be in the place I am today had it not been for their persistent guidance and aid.

This manuscript was submitted on October 18, 2011.

TABLE OF CONTENTS

	Page
ACKNOWLEDGEMENTS	v
LIST OF TABLES	vii
LIST OF FIGURES	viii
CHAPTER	
1. INTRODUCTION	1
2. EXPERIMENTAL METHODS.....	4
2.1. Synthesis and Crystal Growth.....	4
2.2. Wide Angle X-Ray Diffraction.....	6
2.3. Single Crystal X-Ray Diffraction	7
2.4. Data Collection and Reduction for $\text{Fe}(\text{H}_2\text{O})_2\text{Ni}(\text{CN})_4 \cdot 4\text{H}_2\text{O}$	7
2.5. Structure Solution and Refinement of $\text{Fe}(\text{H}_2\text{O})_2\text{Ni}(\text{CN})_4 \cdot 4\text{H}_2\text{O}$	8
2.6. Data Collection and Reduction for $\text{Fe}(\text{H}_2\text{O})_2\text{Ni}(\text{CN})_4 \cdot \text{H}_2\text{O}$	9
2.7. Structure Solution and Refinement of $\text{Fe}(\text{H}_2\text{O})_2\text{Ni}(\text{CN})_4 \cdot \text{H}_2\text{O}$	10
2.8. Data Collection and Reduction for $\text{Cd}(\text{H}_2\text{O})_2\text{Ni}(\text{CN})_4 \cdot 4\text{H}_2\text{O}$	11
2.9. Structure Solution and Refinement of $\text{Cd}(\text{H}_2\text{O})_2\text{Ni}(\text{CN})_4 \cdot 4\text{H}_2\text{O}$	12
2.10 Separation of Individual Layers to Form Nanosheets.....	12
2.11 Scanning Electron Microscopy and Atomic Force Microscopy	13
3. RESULTS AND DISCUSSION	15
3.1. Refinement Results for $\text{Fe}(\text{H}_2\text{O})_2\text{Ni}(\text{CN})_4 \cdot 4\text{H}_2\text{O}$	15
3.2. Refinement Results for $\text{Fe}(\text{H}_2\text{O})_2\text{Ni}(\text{CN})_4 \cdot \text{H}_2\text{O}$	16
3.3. Refinement Results for $\text{Cd}(\text{H}_2\text{O})_2\text{Ni}(\text{CN})_4 \cdot 4\text{H}_2\text{O}$	18
3.4. Structural Description	20
3.5 Wide Angle X-Ray Diffraction Results and Discussion.....	26
3.6 AFM and SEM Morphological Studies of Individual Nanosheets	30
4. CONCLUSION.....	33
REFERENCES	35

LIST OF TABLES

Table	Page
1. Masses of reactants for crystal growth.....	6
2. Crystal data and structure refinement details for $\text{Fe}(\text{H}_2\text{O})_2\text{Ni}(\text{CN})_4 \cdot 4\text{H}_2\text{O}$	15
3. Selected bond lengths for $\text{Fe}(\text{H}_2\text{O})_2\text{Ni}(\text{CN})_4 \cdot 4\text{H}_2\text{O}$	16
4. Crystal data and structure refinement details for $\text{Fe}(\text{H}_2\text{O})_2\text{Ni}(\text{CN})_4 \cdot \text{H}_2\text{O}$	17
5. Selected bond lengths for $\text{Fe}(\text{H}_2\text{O})_2\text{Ni}(\text{CN})_4 \cdot \text{H}_2\text{O}$	18
6. Crystal data and structure refinement details for $\text{Cd}(\text{H}_2\text{O})_2\text{Ni}(\text{CN})_4 \cdot 4\text{H}_2\text{O}$	18
7. Selected bond lengths for $\text{Cd}(\text{H}_2\text{O})_2\text{Ni}(\text{CN})_4 \cdot 4\text{H}_2\text{O}$	19
8. Comparison of experimental single crystal X-ray diffraction bond lengths with molecular modeling predicted bond lengths	24
9. Comparison of experimental single crystal X-ray diffraction bond angles with molecular modeling predicted bond angles	25

LIST OF FIGURES

Figure	Page
1. Crystal growth apparatus	5
2. Projections of $\text{Fe}(\text{H}_2\text{O})_2\text{Ni}(\text{CN})_4 \cdot 4\text{H}_2\text{O}$	21
3. Projections of $\text{Cd}(\text{H}_2\text{O})_2\text{Ni}(\text{CN})_4 \cdot 4\text{H}_2\text{O}$	21
4. Projections of $\text{Fe}(\text{H}_2\text{O})_2\text{Ni}(\text{CN})_4 \cdot \text{H}_2\text{O}$	23
5. TGA of $\text{Fe}(\text{H}_2\text{O})_2\text{Ni}(\text{CN})_4 \cdot 4\text{H}_2\text{O}$	23
6. Molecular model of $\text{Fe}(\text{H}_2\text{O})_2\text{Ni}(\text{CN})_4 \cdot \text{H}_2\text{O}$	25
7. Molecular model of dehydrated $\text{FeNi}(\text{CN})_4$	26
8. Wide angle XRD patterns for the hydrated compounds	27
9. Wide angle XRD patterns showing interlayer expansion	30
10. SEM images of nanosheets.	31
11. AFM analysis of $\text{MnNi}(\text{CN})_4$ nanosheet.....	32

CHAPTER 1

INTRODUCTION

Since the discovery and isolation of graphene in 2004, interest has risen greatly in two-dimensional nanomaterials.^{1,2,3} Two-dimensional materials such as graphene have been shown to possess electrical and magnetic properties unique to their class.^{4,5,6,7,8} These types of properties on such a small scale are essential for the production of nanoscale electronics, the next generation of computing and electronic devices. The separation or exfoliation of individual 2-D sheets from a parent multilayer structure is one method that has been used to prepare suspensions or single layers of 2-D nanoparticles with unique properties different from those of the parent structure.^{9,10,11} Exfoliation is a convenient method of nanosheet production because it enables the rapid production of substantial quantities of the single layer structures from the more easily obtained parent structure. New types of two-dimensional materials produced in this manner are currently sought after to explore the various properties they may exhibit.

Metal cyanide-bridged frameworks such as the pigment Prussian blue have been used in the past for various applications,¹² but more recently such frameworks have been used as polymerization catalysts.^{13,14} Another class of metal cyanide-bridged frameworks is the Hofmann-type clathrates, which have been studied at length in past for their unique structural properties.^{15,16} These compounds are composed of two-dimensional networks

of square planar nickel atoms linked via cyanide bridges to another metal that forms octahedral coordination with the four bridging cyanide ligands and two molecules on either side of the sheet, usually amines. In addition, aromatic interlayer molecules usually occupy space between the layers in a Hofmann-type clathrate. The structures studied and reported here are similar to these clathrates, with the exception that the usual amines and aromatic compounds are not present. Previously, structural studies have been carried out on three similar compounds; $\text{Ni}(\text{H}_2\text{O})_2\text{Ni}(\text{CN})_4 \cdot 4\text{H}_2\text{O}$, $\text{Co}(\text{H}_2\text{O})_2\text{Ni}(\text{CN})_4 \cdot 4\text{H}_2\text{O}$ and $\text{Cd}(\text{H}_2\text{O})_2\text{Ni}(\text{CN})_4 \cdot 4\text{H}_2\text{O}$.^{17,18,19} The single crystal X-ray diffraction studies reported here correspond to an iron(II) variant of these structures and a partially dehydrated iron(II) variant with empirical formulas of $\text{Fe}(\text{H}_2\text{O})_2\text{Ni}(\text{CN})_4 \cdot 4\text{H}_2\text{O}$ and $\text{Fe}(\text{H}_2\text{O})_2\text{Ni}(\text{CN})_4 \cdot \text{H}_2\text{O}$, respectively. Another crystallographic study of $\text{Cd}(\text{H}_2\text{O})_2\text{Ni}(\text{CN})_4 \cdot 4\text{H}_2\text{O}$ is also presented. In general, a structure of this type with varying octahedrally coordinated metals will be referred to as $\text{M}(\text{H}_2\text{O})_2\text{Ni}(\text{CN})_4 \cdot 4\text{H}_2\text{O}$, where M can refer to various transition metals. In addition to the single crystal x-ray diffraction studies, powder X-ray diffraction studies have been carried out on compounds where M is Mn, Fe, Co, Cd, Ni, or Zn, all in the +2 valence state.

Previously, calculations have been carried out by Dr. Byounghak Lee and Craig Higgins of Texas State University–San Marcos to predict the electronic and magnetic properties of a dehydrated monolayer of this type of compound with the empirical formula $\text{MNi}(\text{CN})_4$.²⁰ The predictions showed that these compounds may possess unusual magnetic and conductor properties and that the properties can be altered depending on the type of metal placed in the M position. At the time, when these calculations were carried

out, no method had been developed to isolate the single molecular layers for which the DFT calculations had been performed.

The second portion of this study reports on a novel method of separation of individual nanosheets from the parent multilayer structure. Recently, work has been carried out using Langmuir-Blodgett techniques to create single two-dimensional layers of Fe^{3+} - Ni^{2+} square grid cyanide networks at the air-water interface and measure the magnetic properties of such a monolayer.^{21,22,23} This monolayer requires a ligand on the Fe^{3+} atom to balance the charge and induce the hydrophobic properties required for the technique. No method has ever been previously reported to separate a single nanosheet of a ligand-free, dehydrated M^{2+} - Ni^{2+} cyanide-bridged network from its parent structure. It has been shown previously that dodecyl pyrrolidone (DDP) will substitute for interlayer water molecules in montmorillonite,²⁴ and this type of phenomenon also occurs in other sheet-like multilayer structures.^{25,26} In this study, a novel method is presented in which replacement of dodecyl pyrrolidone (DDP) for the interlayer water molecules has been utilized to push apart and completely exfoliate individual nanosheets of various $\text{MNi}(\text{CN})_4$ compounds. Powder X-ray diffraction studies monitor the expansion of the layers as the interlayer molecules change. Scanning electron microscopy (SEM) and atomic force microscopy (AFM) have been utilized to verify the morphology and thickness of these exfoliated single layers.

CHAPTER 2

EXPERIMENTAL METHODS

2.1 Synthesis and Crystal Growth

Two methods of synthesis were used to prepare the $M(H_2O)_2Ni(CN)_4 \cdot 4H_2O$ compounds. Bulk material in powder form was prepared initially. In a typical bulk precipitation, equimolar amounts of potassium tetracyanonickelate(II) hydrate (Aldrich) and a salt of the desired metal were added together into aqueous solution, with the solid metal salt added to an aqueous potassium tetracyanonickelate(II) hydrate solution. Upon addition, a fine precipitate was observed to form. The precipitate was then washed to remove any excess reactants. This washing was conducted by centrifugation using an Allegra® 6 Benchtop Centrifuge and decanting the supernatant liquid from the precipitated product three times. After each centrifugation, the supernatant liquid was decanted, and 200 mL of deionized water was added to the centrifuge bottle to dissolve remaining reactants. The resulting washed precipitated product was then placed under a stream of air at room temperature until dry. The product was determined to be dry when the product was a solid powder rather than a wet paste. The metal salts used in the preparation of these compounds were iron(II) ammonium sulfate hexahydrate (SchalAR Chemistry, reagent grade), anhydrous manganese(II) chloride (Alfa Aesar, 97%), cobalt

chloride hexahydrate (Sigma-Aldrich, 98%), nickel sulfate hexahydrate (Alfa Aesar, 98%), cadmium(II) chloride hydrate (Alfa Aesar, 99%), and anhydrous zinc chloride (Spectrum, 97%). Dehydrated compounds were prepared by heating the original product to 180 °C in an oven for 24 hours in air. The dehydration temperature was determined by thermogravimetric analysis (TGA) on a TA Instruments Q50. The TGA data was acquired at a range of 35.00 °C to 250.00 °C at a temperature ramp of 10.00 °C/min in air.

Crystals of several $M(H_2O)_2Ni(CN)_4 \cdot 4H_2O$ compounds were grown by slow diffusion of reactants through a water bridge. An aqueous solution of each reactant of was placed in a test tube, one containing a salt of the desired metal and the other containing potassium tetracyanonickelate(II) hydrate (Aldrich). The two solutions were of equal molar concentration. The two tubes were then connected by a water bridge and sealed using rubber stoppers with holes for the water bridge. The tubes were then placed in an oven at 40 °C to encourage diffusion through the bridge. Crystal formation was observed after several weeks. An illustration of the apparatus is shown in Figure 1.

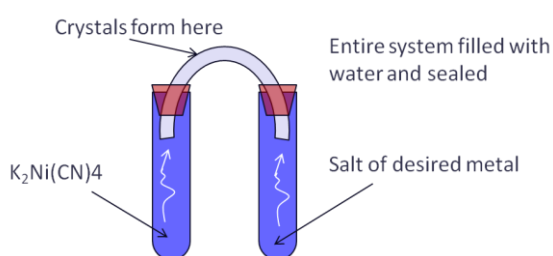


Figure 1. Crystal growth apparatus. This illustrates the apparatus used to grow crystals for each compound. Each reactant slowly diffuses into the water bridge, forming crystals at the junction.

Systems of this type were prepared for several different M metal types using varying concentrations of reactants. Tubes of three different concentrations for each metal type

were prepared to determine the effect of concentration on crystal growth. In general, the systems with higher concentration exhibited more prolific crystal growth, but the few crystals that did grow at lower concentrations were easier to isolate and were less crowded. Often, the crystals grown at higher concentration would grow closer together in clusters, proving separation difficult. The amounts of reactant used in each tube are given in Table 1. The mature crystals were gently rinsed with deionized water and kept in vials containing deionized water at room temperature to prevent dehydration and splitting.

Table 1. Masses of reactants for crystal growth. The masses of reactants used in each system for crystal growth are given, along with the type of salt used for each variation.

Compound	Metal Salt	Mass of Metal Salt (g)	Mass of $\text{K}_2\text{Ni}(\text{CN})_4 \cdot x\text{H}_2\text{O}$ (g)
$\text{Co}(\text{H}_2\text{O})_2\text{Ni}(\text{CN})_4 \cdot 4\text{H}_2\text{O}$	$\text{CoCl}_2 \cdot 6\text{H}_2\text{O}$	0.0987	0.1098
		0.0490	0.0566
		0.0244	0.0288
$\text{Fe}(\text{H}_2\text{O})_2\text{Ni}(\text{CN})_4 \cdot 4\text{H}_2\text{O}$	$\text{Fe}(\text{NH}_4)_2(\text{SO}_4)_2 \cdot 6\text{H}_2\text{O}$ (SchalAR Chemistry, reagent grade)	0.1634	0.0999
		0.0814	0.0505
		0.0410	0.0252
$\text{Zn}(\text{H}_2\text{O})_2\text{Ni}(\text{CN})_4 \cdot 4\text{H}_2\text{O}$	ZnCl_2	0.1141	0.1972
		0.0523	0.1025
		0.0343	0.0553
$\text{Mn}(\text{H}_2\text{O})_2\text{Ni}(\text{CN})_4 \cdot 4\text{H}_2\text{O}$	MnCl_2 (Alfa Aesar, 97%)	0.1113	0.1984
		0.0602	0.1035
		0.0258	0.0530
$\text{Cd}(\text{H}_2\text{O})_2\text{Ni}(\text{CN})_4 \cdot 4\text{H}_2\text{O}$	CdCl_2	0.1522	0.1997
		0.0678	0.0950
		0.0448	0.0582

2.2 Wide Angle X-ray Diffraction

All wide angle X-ray diffraction measurements were carried out using a Bruker D8 Focus diffractometer using a Cu $K\alpha$ radiation source. The powder products synthesized via the bulk precipitation method were used for powder XRD.

2.3 Single Crystal X-ray Diffraction

Single crystal X-ray diffraction data were collected using a Rigaku Mercury275R CCD (SCX Mini) diffractometer using graphite monochromated Mo-K α radiation. Crystallographic equipment was acquired through the support of the National Science Foundation (CHE-0821254). Crystals of Fe(H₂O)₂Ni(CN)₄·4H₂O and Cd(H₂O)₂Ni(CN)₄·4H₂O were grown using the tube system previously described. The best quality crystal was chosen for each compound. The Fe(H₂O)₂Ni(CN)₄·4H₂O crystal was mounted on a fiber, and data were collected at a temperature of 20.0 °C. The Cd(H₂O)₂Ni(CN)₄·4H₂O crystal was mounted on a fiber, and data were collected at -50.0 °C under a stream of nitrogen. To collect data for Fe(H₂O)₂Ni(CN)₄·H₂O, a high quality Fe(H₂O)₂Ni(CN)₄·4H₂O crystal was placed in a capillary tube and heated to 50 °C for 24 hours. The capillary tube was then sealed, and data were collected at a temperature of 20.0 °C. Single crystal X-ray diffraction data of a fully dehydrated crystal could not be obtained. Most of the crystals fell apart upon dehydration, and the successfully mounted crystals had a high degree of disorder and were not suitable for single crystal X-ray crystallography.

2.4 Data Collection and Reduction for Fe(H₂O)₂Ni(CN)₄·4H₂O

The data were collected to a maximum 2 θ value of 55.0°. A total of 540 oscillation images were collected. A sweep of data was done using ω scans from -120.0 to 60.0° in 1.0° step, at χ =54.0° and ϕ = 0.0°. The exposure rate was 10.0 [sec./°]. The detector swing angle was -29.90°. A second sweep was performed using ω scans from -

120.0 to 60.0° in 1.0° step, at $\chi=54.0^\circ$ and $\phi = 120.0^\circ$. The exposure rate was 10.0 [sec./°]. The detector swing angle was -29.90° . Another sweep was performed using ω scans from -120.0 to 60.0° in 1.0° step, at $\chi=54.0^\circ$ and $\phi = 240.0^\circ$. The exposure rate was 10.0 [sec./°]. The detector swing angle was -29.90° . The crystal-to-detector distance was 51.00 mm. Readout was performed in the 0.146 mm pixel mode.

Of the 11906 reflections that were collected, 1465 were unique ($R_{\text{int}} = 0.0240$); equivalent reflections were merged. Data were collected and processed using CrystalClear (Rigaku).²⁷

The linear absorption coefficient, μ , for Mo-K α radiation is 27.403 cm^{-1} . An empirical absorption correction was applied which resulted in transmission factors ranging from 0.236 to 0.405. The data were corrected for Lorentz and polarization effects.

2.5 Structure Solution and Refinement of $\text{Fe}(\text{H}_2\text{O})_2\text{Ni}(\text{CN})_4 \cdot 4\text{H}_2\text{O}$

The structure was solved by heavy-atom Patterson methods²⁸ and expanded using Fourier techniques. The non-hydrogen atoms were refined anisotropically. Some hydrogen atoms were located but were excluded from the final refinement due to uncertainty of their correct positions. The final cycle of full-matrix least-squares refinement on F was based on 1409 observed reflections ($I > 2.00\sigma(I)$) and 79 variable parameters and converged (largest parameter shift was 0.00 times its esd) with unweighted and weighted agreement factors of:

$$R = \Sigma ||F_o| - |F_c|| / \Sigma |F_o| = 0.0285$$

$$R_w = [\sum w (|F_o| - |F_c|)^2 / \sum w F_o^2]^{1/2} = 0.0260$$

The standard deviation of an observation of unit weight was 0.95. A Robust-resistant weighting scheme was used.²⁹ Plots of $\sum w (|F_o| - |F_c|)^2$ versus $|F_o|$, reflection order in data collection, $\sin \theta/\lambda$ and various classes of indices showed no unusual trends. The maximum and minimum peaks on the final difference Fourier map corresponded to 0.83 and -0.88 e⁻/Å³, respectively.

The following applies to the solution and refinement of Cd(H₂O)₂Ni(CN)₄·4H₂O, Fe(H₂O)₂Ni(CN)₄·4H₂O, and Fe(H₂O)₂Ni(CN)₄·H₂O. Neutral atom scattering factors were taken from Cromer and Waber.³⁰ Anomalous dispersion effects were included in F_{calc}³¹; the values for $\Delta f'$ and $\Delta f''$ were those of Creagh and McAuley.³² The values for the mass attenuation coefficients are those of Creagh and Hubbell.³³ All calculations were performed using the CrystalStructure^{34,35} crystallographic software package.

2.6 Data Collection and Reduction for Fe(H₂O)₂Ni(CN)₄·H₂O

The data were collected to a maximum 2 θ value of 54.9°. A total of 540 oscillation images were collected. A sweep of data was done using ω scans from -120.0 to 60.0° in 1.0° step, at χ =54.0° and ϕ = 0.0°. The exposure rate was 30.0 [sec./°]. The detector swing angle was -29.90°. A second sweep was performed using ω scans from -120.0 to 60.0° in 1.0° step, at χ =54.0° and ϕ = 120.0°. The exposure rate was 30.0 [sec./°]. The detector swing angle was -29.90°. Another sweep was performed using ω scans from -120.0 to 60.0° in 1.0° step, at χ =54.0° and ϕ = 240.0°. The exposure rate

was 30.0 [sec./°]. The detector swing angle was -29.90°. The crystal-to-detector distance was 51.00 mm. Readout was performed in the 0.146 mm pixel mode.

Of the 4510 reflections that were collected, 593 were unique ($R_{\text{int}} = 0.0548$); equivalent reflections were merged. Data were collected and processed using CrystalClear (Rigaku).²⁷

The linear absorption coefficient, μ , for Mo-K α radiation is 35.692 cm⁻¹. An empirical absorption correction was applied which resulted in transmission factors ranging from 0.423 to 0.629. The data were corrected for Lorentz and polarization effects.

2.7 Structure Solution and Refinement of Fe(H₂O)₂Ni(CN)₄·H₂O

The structure was solved by direct methods²⁸ and expanded using Fourier techniques. The non-hydrogen atoms were refined anisotropically. Hydrogen atoms were not located. The final cycle of full-matrix least-squares refinement on F was based on 546 observed reflections ($I > 2.00\sigma(I)$) and 37 variable parameters and converged (largest parameter shift was 0.00 times its esd) with unweighted and weighted agreement factors of:

$$R = \sum ||F_o| - |F_c|| / \sum |F_o| = 0.0475$$

$$R_w = [\sum w (|F_o| - |F_c|)^2 / \sum w F_o^2]^{1/2} = 0.0543$$

The standard deviation of an observation of unit weight was 1.08. A Robust-resistant weighting scheme was used.²⁹ Plots of $\sum w (|F_o| - |F_c|)^2$ versus $|F_o|$, reflection order in data collection, $\sin \theta/\lambda$ and various classes of indices showed no unusual trends.

The maximum and minimum peaks on the final difference Fourier map corresponded to 1.37 and -1.40 e⁻/Å³, respectively.

2.8 Data Collection and Reduction for Cd(H₂O)₂Ni(CN)₄·4H₂O

The data were collected to a maximum 2θ value of 55.0°. A total of 540 oscillation images were collected. A sweep of data was done using ω scans from -120.0 to 60.0° in 1.0° step, at χ = 54.0° and φ = 0.0°. The exposure rate was 20.0 [sec./°]. The detector swing angle was -29.90°. A second sweep was performed using ω scans from -120.0 to 60.0° in 1.0° step, at χ = 54.0° and φ = 120.0°. The exposure rate was 20.0 [sec./°]. The detector swing angle was -29.90°. Another sweep was performed using ω scans from -120.0 to 60.0° in 1.0° step, at χ = 54.0° and φ = 240.0°. The exposure rate was 20.0 [sec./°]. The detector swing angle was -29.90°. The crystal-to-detector distance was 51.00 mm. Readout was performed in the 0.146 mm pixel mode.

Of the 12625 reflections that were collected, 1554 were unique (R_{int} = 0.0240); equivalent reflections were merged. Data were collected and processed using CrystalClear (Rigaku).²⁷

The linear absorption coefficient, μ, for Mo-Kα radiation is 30.846 cm⁻¹. An empirical absorption correction was applied which resulted in transmission factors ranging from 0.378 to 0.540. The data were corrected for Lorentz and polarization effects.

2.9 Structure Solution and Refinement of $\text{Cd}(\text{H}_2\text{O})_2\text{Ni}(\text{CN})_4 \cdot 4\text{H}_2\text{O}$

The structure was solved by heavy-atom Patterson methods²⁸ and expanded using Fourier techniques. The non-hydrogen atoms were refined anisotropically. Some hydrogen atoms were located but were excluded from the final refinement due to uncertainty of their correct positions. The final cycle of full-matrix least-squares refinement on F was based on 1554 observed reflections ($I > 0.00s(I)$) and 79 variable parameters and converged (largest parameter shift was 0.00 times its esd) with unweighted and weighted agreement factors of:

$$R = \sum ||F_o| - |F_c|| / \sum |F_o| = 0.0398$$

$$R_w = [\sum w (|F_o| - |F_c|)^2 / \sum w F_o^2]^{1/2} = 0.0256$$

The standard deviation of an observation of unit weight was 1.04. A Robust-resistant weighting scheme was used.²⁹ Plots of $\sum w (|F_o| - |F_c|)^2$ versus $|F_o|$, reflection order in data collection, $\sin \theta/\lambda$, and various classes of indices showed no unusual trends. The maximum and minimum peaks on the final difference Fourier map corresponded to 1.52 and -1.82 $\text{e}^-/\text{\AA}^3$, respectively.

2.10 Separation of Individual Layers to Form Nanosheets

A process was developed to intercalate with dodecyl pyrrolidone (DDP), exfoliate, and isolate individual sheets consisting of a single molecular layer. DDP was used to replace the interlayer water molecules and expand the distance between layers. The DDP was manufactured by International Specialty Products, Inc. under the trade name Surfadone® LP-300. An intercalated product was prepared first to demonstrate that

intercalation can occur in these compounds. The powder $\text{Fe}(\text{H}_2\text{O})_2\text{Ni}(\text{CN})_4 \cdot 4\text{H}_2\text{O}$ product was placed in a vial, and DDP was added until the powder was saturated with the liquid to obtain a paste. The vial was then heated to 175 °C and held at that temperature for one hour. After sitting in air for 24 hours, any excess DDP was wiped away from the brown paste.

To separate individual sheets, suspensions exfoliated in DDP were prepared using crystals prepared via the tube system described previously. Multiple crystals of the same type, ranging in size from about 0.2 mm to 0.8 mm, were placed into a vial containing 5 mL of DDP and heated in an oven to a temperature of 175 °C. As the temperature approached 175 °C, the crystals were observed to be expanding, and then falling apart in sheet-like pieces. After allowing the contents of the vial to cool to room temperature, the DDP suspension was sonicated using an ultrasonic horn. The suspension was sonicated for two 30 second intervals, allowing the suspension to cool to room temperature between intervals. This process was carried out for compounds with Co^{2+} , Fe^{2+} , and Mn^{2+} in the M position.

2.11 Scanning Electron Microscopy and Atomic Force Microscopy

Samples were prepared for both SEM and AFM. Using the DDP suspensions prepared from exfoliated single crystals, nanosheets were deposited onto different substrates. AFM images were collected on a mica substrate, and SEM images were collected on a silicon substrate. Both substrates were cut to 1 cm by 1 cm squares before deposition. First, the DDP suspensions were sonicated for five seconds to ensure uniform dispersion. A small droplet of the suspension was placed onto the desired substrate then

heated to 180 °C under vacuum. This temperature was held for one hour to drive off any remaining DDP. All samples were heated to 180 °C and placed in a desiccator to ensure dehydration of the nanosheets prior to imaging. SEM imaging was performed using a Helios NanoLab 400 from FEI Company. SEM equipment was acquired through the support of the National Science Foundation (Award #0923509). AFM imaging was performed using a Veeco Dimension 3100 microscope in tapping mode using Veeco ULNC-AUHW type “B” cantilevers.

CHAPTER 3

RESULTS AND DISCUSSION

3.1 Refinement Results for $\text{Fe}(\text{H}_2\text{O})_2\text{Ni}(\text{CN})_4 \cdot 4\text{H}_2\text{O}$

The crystalline $\text{Fe}(\text{H}_2\text{O})_2\text{Ni}(\text{CN})_4 \cdot 4\text{H}_2\text{O}$ structure was found to be in the orthorhombic *Pnma* space group. The unit cell parameters are $a = 12.0962(7)$ Å, $b = 14.0037(8)$ Å, and $c = 7.2250(4)$ Å. A list of the structural refinement and data collection parameters for $\text{Fe}(\text{H}_2\text{O})_2\text{Ni}(\text{CN})_4 \cdot 4\text{H}_2\text{O}$ are shown in Table 2. Hydrogen atoms were excluded from the final refinement due to the uncertainty of their positions. A list of selected bond lengths is given in Table 3.

Table 2. Crystal data and structure refinement details for $\text{Fe}(\text{H}_2\text{O})_2\text{Ni}(\text{CN})_4 \cdot 4\text{H}_2\text{O}$.

Empirical Formula	$\text{C}_4\text{H}_{12}\text{FeN}_4\text{NiO}_6$
Formula Weight	326.71
Crystal Color, Habit	colorless, prism
Temperature	20.0°C
Crystal Dimensions	0.79 X 0.45 X 0.33 mm
Crystal System	Orthorhombic
Lattice Type	Primitive
Lattice Parameters	$a = 12.0962(7)$ Å $b = 14.0037(8)$ Å $c = 7.2250(4)$ Å $V = 1223.86(12)$ Å ³
Space Group	<i>Pnma</i> (#62)
Z value	4

Table 2-Continued	
Dcalc	1.773 g/cm ³
F(000)	664
$\mu(\text{MoK}\alpha)$	27.403 cm ⁻¹
Reflections Collected	11906
Independent Reflections	1465 (Rint = 0.0240)
Observations (I>2.00 σ (I))	1409
Variables	79
Reflection/Parameter Ratio	17.84
Refinement Method	Full-matrix least-squares on F
Function Minimized	$\sum w (F_o - F_c)^2$
Least Squares Weights	Chebyshev polynomial with 3 parameters 3.6881, 0.7577, 2.4643
$2\theta_{\text{max}}$ cutoff	55.0°
Anomalous Dispersion	All non-hydrogen atoms
Residuals: R (I>2.00 σ (I))	0.0285
Residuals: wR (I>2.00 σ (I))	0.0260
Goodness of Fit Indicator	0.955
Max Shift/Error in Final Cycle	0.000
Maximum peak in Final Diff. Map	0.83 e-/Å ³
Minimum peak in Final Diff. Map	-0.88 e-/Å ³

Table 3. Selected bond lengths
for Fe(H₂O)₂Ni(CN)₄·4H₂O.

Atom 1	Atom 2	Distance (Å)
Ni(1)	C(1)	1.8627(11)
Ni(1)	C(2)	1.8609(11)
Fe(1)	O(1)	2.1561(9)
Fe(1)	N(1)	2.1386(11)
Fe(1)	N(2)	2.1432(11)
N(1)	C(1)	1.1464(16)
N(2)	C(2)	1.1502(16)

3.2 Refinement Results for Fe(H₂O)₂Ni(CN)₄·H₂O

The crystalline Fe(H₂O)₂Ni(CN)₄·H₂O structure was found to be in the orthorhombic *Imma* space group. The unit cell parameters are $a = 7.2153(10)$ Å, $b =$

14.3801(18) Å, and $c = 8.9471(12)$ Å. A list of the structural refinement and data collection parameters for $\text{Fe}(\text{H}_2\text{O})_2\text{Ni}(\text{CN})_4 \cdot \text{H}_2\text{O}$ are shown in Table 4.

Table 4. Crystal data and structure refinement details for $\text{Fe}(\text{H}_2\text{O})_2\text{Ni}(\text{CN})_4 \cdot \text{H}_2\text{O}$

Empirical Formula	$\text{C}_4\text{H}_6\text{FeN}_4\text{NiO}_3$
Formula Weight	272.66
Crystal Color, Habit	colorless, prism
Temperature	20.0°C
Crystal Dimensions	0.27 X 0.22 X 0.13 mm
Crystal System	Orthorhombic
Lattice Type	I-centered
Lattice Parameters	$a = 7.2153(10)$ Å $b = 14.3801(18)$ Å $c = 8.9471(12)$ Å $V = 928.3(2)$ Å ³
Space Group	Imma (#74)
Z value	4
Dcalc	1.951 g/cm ³
F(000)	544
$\mu(\text{MoK}\alpha)$	35.692 cm ⁻¹
Reflections Collected	4510
Independent Reflections	593 (Rint = 0.0548)
Observations ($I > 2.00\sigma(I)$)	546
Variables	37
Reflection/Parameter Ratio	14.76
Refinement	Full-matrix least-squares on F
Function Minimized	$\sum w (F_o - F_c)^2$
Least Squares Weights	Chebyshev polynomial with 3 parameters 6.2750, 0.8991, 4.6084
$2\theta_{\text{max}}$ cutoff	54.9°
Anomalous Dispersion	All non-hydrogen atoms
Residuals: R ($I > 2.00\sigma(I)$)	0.0475
Residuals: wR ($I > 2.00\sigma(I)$)	0.0543
Goodness of Fit Indicator	1.083
Max Shift/Error in Final Cycle	0.000
Maximum peak in Final Diff. Map	1.37 e-/Å ³
Minimum peak in Final Diff. Map	-1.40 e-/Å ³

The hydrogen atoms could not be located from the difference map. A list of selected bond lengths is given in Table 5.

Table 5. Selected bond lengths for $\text{Fe}(\text{H}_2\text{O})_2\text{Ni}(\text{CN})_4\cdot\text{H}_2\text{O}$.

Atom 1	Atom 2	Distance (Å)
Ni(1)	C(1)	1.861(3)
Fe(1)	N(1)	2.128(3)
Fe(1)	O(1)	2.196(5)
N(1)	C(1)	1.150(5)

3.3 Refinement Results for $\text{Cd}(\text{H}_2\text{O})_2\text{Ni}(\text{CN})_4\cdot 4\text{H}_2\text{O}$

The crystalline $\text{Cd}(\text{H}_2\text{O})_2\text{Ni}(\text{CN})_4\cdot 4\text{H}_2\text{O}$ structure was found to be in the orthorhombic *Pnma* space group. The unit cell parameters are $a = 12.3358(12)$ Å, $b = 14.2754(14)$ Å, and $c = 7.4275(7)$ Å. As one might expect, the unit cell for the reported $\text{Cd}(\text{H}_2\text{O})_2\text{Ni}(\text{CN})_4\cdot 4\text{H}_2\text{O}$ variation is slightly larger than that of the iron(II) compound due to the larger radius of the Cd^{2+} ion. A list of the structural refinement and data collection parameters for $\text{Cd}(\text{H}_2\text{O})_2\text{Ni}(\text{CN})_4\cdot 4\text{H}_2\text{O}$ are shown in Table 6. The hydrogen atoms were excluded from the final refinement due to the uncertainty of their positions. A list of selected bond lengths is given in Table 7.

Table 6. Crystal data and structure refinement details for $\text{Cd}(\text{H}_2\text{O})_2\text{Ni}(\text{CN})_4\cdot 4\text{H}_2\text{O}$.

Empirical Formula	$\text{C}_4\text{H}_{12}\text{CdN}_4\text{NiO}_6$
Formula Weight	383.27
Crystal Color, Habit	colorless, prism
Temperature	-50.0°C
Crystal Dimensions	0.49 X 0.33 X 0.20 mm
Crystal System	Orthorhombic
Lattice Type	Primitive
Lattice Parameters	$a = 12.3358(12)$ Å $b = 14.2754(14)$ Å $c = 7.4275(7)$ Å

Table 6-Continued

	$V = 1308.0(2) \text{ \AA}^3$
Space Group	Pnma (#62)
Z value	4
Dcalc	1.946 g/cm^3
F(000)	752
$\mu(\text{MoK}\alpha)$	30.846 cm^{-1}
Reflections Collected	12625
Independent Reflections	1554 (Rint = 0.0240)
Observations	1554
Variables	79
Reflection/Parameter Ratio	19.67
Refinement	Full-matrix least-squares on F
Function Minimized	$\sum w (F_o - F_c)^2$
Least Squares Weights	Chebyshev polynomial with 3 parameters 2.0010, 0.5080, 0.1345
$2\theta_{\text{max}}$ cutoff	55.0°
Anomalous Dispersion	All non-hydrogen atoms
Residuals: R ($I > 2.00\sigma(I)$)	0.0398
Residuals: R (All reflections)	0.0412
Residuals: wR (All reflections)	0.0256
Goodness of Fit Indicator	1.042
Max Shift/Error in Final Cycle	0.000
Maximum peak in Final Diff. Map	1.52 e-/\AA^3
Minimum peak in Final Diff. Map	-1.82 e-/\AA^3

Table 7. Selected bond lengths for $\text{Cd}(\text{H}_2\text{O})_2\text{Ni}(\text{CN})_4 \cdot 4\text{H}_2\text{O}$.

Atom 1	Atom 2	Distance (\AA)
Cd(1)	O(1)	2.3626(19)
Cd(1)	N(1)	2.281(2)
Cd(1)	N(2)	2.280(2)
Ni(1)	C(1)	1.855(2)
Ni(1)	C(2)	1.864(2)
N(1)	C(1)	1.147(3)
N(2)	C(2)	1.143(3)

3.4 Structural Description

The structures of both $\text{Fe}(\text{H}_2\text{O})_2\text{Ni}(\text{CN})_4 \cdot 4\text{H}_2\text{O}$ and $\text{Cd}(\text{H}_2\text{O})_2\text{Ni}(\text{CN})_4 \cdot 4\text{H}_2\text{O}$ were found to consist of two-dimensional sheets with a network of hydrogen-bonded water molecules between the layers. From the similarities between this structure and that of the previously reported $\text{Co}(\text{H}_2\text{O})_2\text{Ni}(\text{CN})_4 \cdot 4\text{H}_2\text{O}$ and $\text{Cd}(\text{H}_2\text{O})_2\text{Ni}(\text{CN})_4 \cdot 4\text{H}_2\text{O}$ structures, the hydrogen atoms are most likely oriented in the same manner as those reported by Niu, et al and Ham, et al, in which the water molecules hydrogen bond in a distorted hexagonal structure between layers.^{18,19} This supposition is made based on the fact that the previously reported structures are isostructural to the structures reported in this study. The d^8 nickel(II) coordinates with the carbon side of four cyanide ligands in a low-spin square planar configuration. One of the water molecules is very weakly bound to the Ni^{2+} center. Both the cadmium(II) and iron(II) metals in each variant were found to coordinate with the nitrogen of four cyanide ligands in a plane with one water molecule on either side of the sheet to form octahedral coordination. The $\text{Cd} \cdots \text{O}$ distance was 2.3626(19) Å, and the $\text{Fe} \cdots \text{O}$ distance was 2.1561(9) Å. A ball and stick projection of $\text{Fe}(\text{H}_2\text{O})_2\text{Ni}(\text{CN})_4 \cdot 4\text{H}_2\text{O}$ down the *c*-axis is shown in Figure 2A, and a projection of the compound showing the square planar and octahedral coordination is shown in Figure 2B. Two similar images are shown for $\text{Cd}(\text{H}_2\text{O})_2\text{Ni}(\text{CN})_4 \cdot 4\text{H}_2\text{O}$ in Figures 3A and 3B.

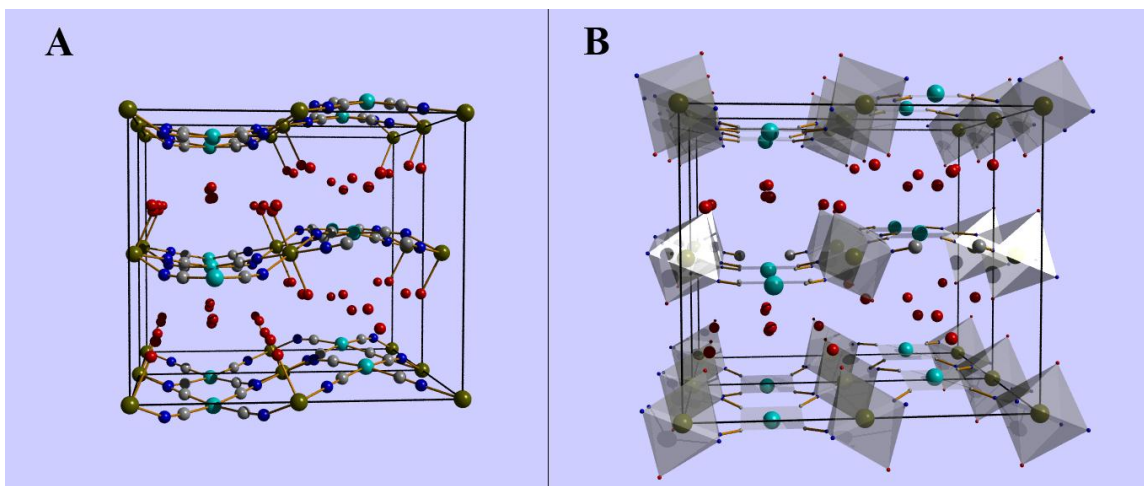


Figure 2. Projections of $\text{Fe}(\text{H}_2\text{O})_2\text{Ni}(\text{CN})_4 \cdot 4\text{H}_2\text{O}$. A (A) ball and stick projection of $\text{Fe}(\text{H}_2\text{O})_2\text{Ni}(\text{CN})_4 \cdot 4\text{H}_2\text{O}$ down the c -axis is shown along with a (B) representation of the octahedral and square planar coordination down the same axis. The unit cell is denoted by the black lines around the structures.

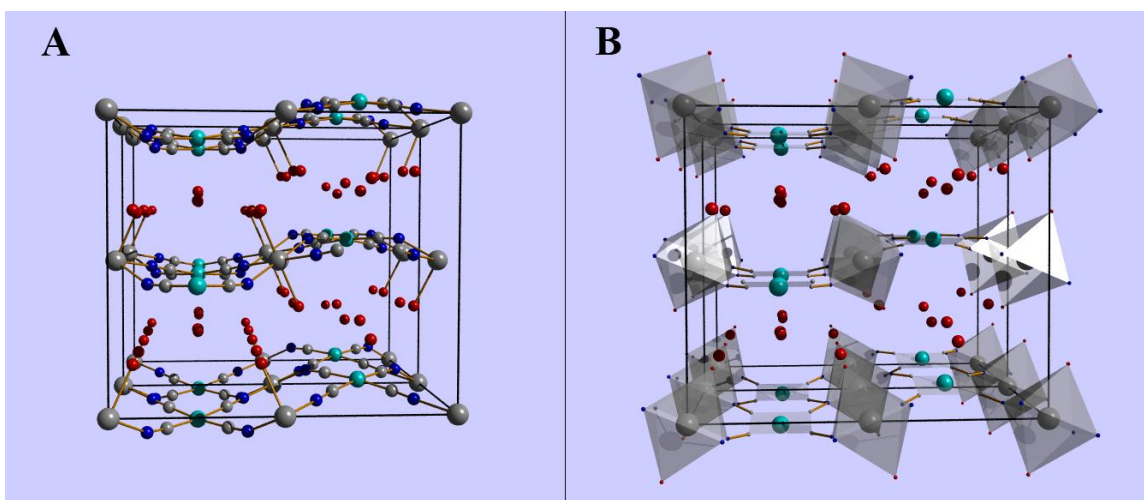


Figure 3. Projections of $\text{Cd}(\text{H}_2\text{O})_2\text{Ni}(\text{CN})_4 \cdot 4\text{H}_2\text{O}$. A (A) ball and stick projection of $\text{Cd}(\text{H}_2\text{O})_2\text{Ni}(\text{CN})_4 \cdot 4\text{H}_2\text{O}$ down the c -axis is shown along with a (B) representation of the octahedral and square planar coordination down the same axis. The unit cell is denoted by the black lines around the structures.

The structure of $\text{Fe}(\text{H}_2\text{O})_2\text{Ni}(\text{CN})_4 \cdot \text{H}_2\text{O}$ consists of a two-dimensional sheet framework similar to that of $\text{Fe}(\text{H}_2\text{O})_2\text{Ni}(\text{CN})_4 \cdot 4\text{H}_2\text{O}$. One difference in the trihydrate structure is the alignment of the sheet curvature to one another. In the fully hydrated

structure, the curvature of a sheet mimics that of the sheet above and below it. In the trihydrate, the curvature of a sheet is opposite that of the sheets above and below as a result of removal of three of the interlayer water molecules. In the trihydrate, two of the water molecules are coordinated to the Fe^{2+} atoms with an $\text{Fe}\cdots\text{O}$ distance of 2.196(5) Å, and the remaining water is weakly attracted to the Ni^{2+} atom with an $\text{Ni}\cdots\text{O}$ distance of 3.089(9) Å. This water molecule is also involved in hydrogen bonding, with the Fe^{2+} coordinated water molecules on either side of it along the *b*-axis as H-donors ($\text{O}\cdots\text{O}$ distance 2.9748(44) Å). A ball and stick projection of $\text{Fe}(\text{H}_2\text{O})_2\text{Ni}(\text{CN})_4\cdot\text{H}_2\text{O}$ down the *a*-axis is shown in Figure 4A, and a projection of the same compound showing the square planar and octahedral coordination is shown in Figure 4B. Thermogravimetric analysis of the fully hydrated iron compound, shown in Figure 5, reveals three regions of weight loss corresponding to the interlayer water molecules. The ratio of weight lost for the first, second and third regions is approximately 3:1:2, respectively. Based on the structure of $\text{Fe}(\text{H}_2\text{O})_2\text{Ni}(\text{CN})_4\cdot\text{H}_2\text{O}$, the first loss is that of the three water molecules held predominantly only by hydrogen bonding. The second loss is that of the single water molecule that is held both by hydrogen bonding and interaction with the Ni^{2+} center. This supports the fact that this water molecule interacts with the Ni^{2+} center. Had there been no interaction with the Ni^{2+} center, this water molecule would have left the interlayer with the first three water molecules, only showing two regions of water loss. The final loss corresponds to the two water molecules held most strongly in the structure by coordination with the Fe^{2+} center.

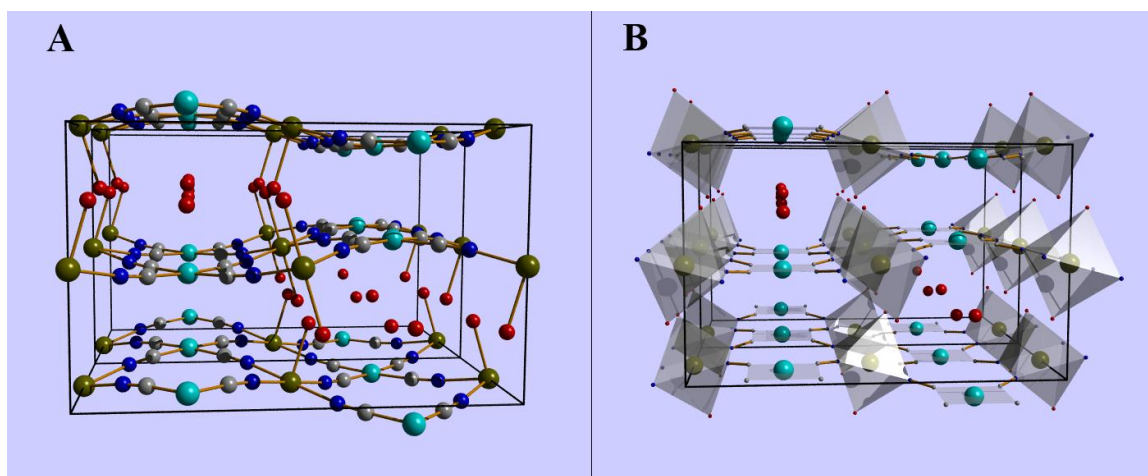


Figure 4. Projections of $\text{Fe}(\text{H}_2\text{O})_2\text{Ni}(\text{CN})_4 \cdot \text{H}_2\text{O}$. A (A) ball and stick projection of $\text{Fe}(\text{H}_2\text{O})_2\text{Ni}(\text{CN})_4 \cdot \text{H}_2\text{O}$ down the a -axis is shown along with a (B) representation of the octahedral and square planar coordination down the same axis. The unit cell is denoted by the black lines around the structures.

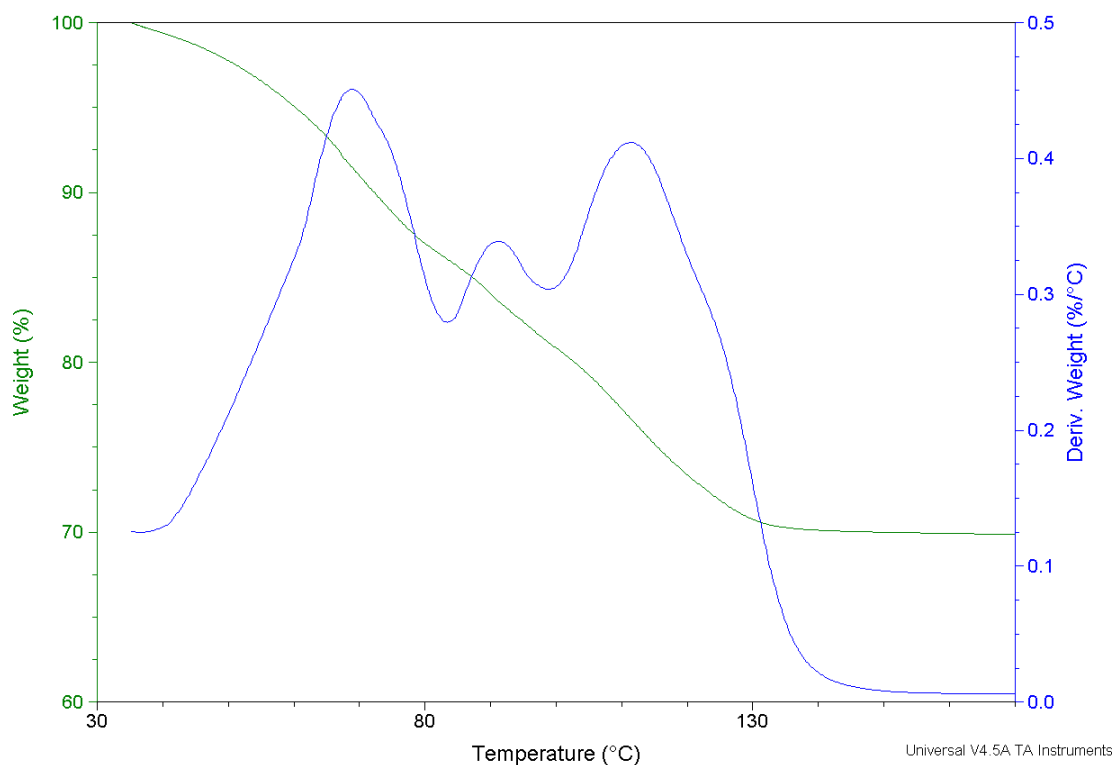


Figure 5. TGA of $\text{Fe}(\text{H}_2\text{O})_2\text{Ni}(\text{CN})_4 \cdot 4\text{H}_2\text{O}$. A TGA plot for $\text{Fe}(\text{H}_2\text{O})_2\text{Ni}(\text{CN})_4 \cdot 4\text{H}_2\text{O}$ is shown with weight percent and derivative of weight percent loss curves. Three regions of loss can be seen, corresponding to the three states of hydration.

These two-dimensional sheets have a slight curvature to accommodate the octahedral and interlayer water molecules. As can be seen in the partially dehydrated structure, $\text{Fe}(\text{H}_2\text{O})_2\text{Ni}(\text{CN})_4\cdot\text{H}_2\text{O}$, the angle of curvature begins to flatten as the interlayer water molecules are removed. Most likely, upon dehydration, the sheets may completely flatten as the strain is removed. Molecular modeling using the Universal force field module in Cerius² by Accelrys®, Inc. was used to predict the structural nature of the completely dehydrated compound. First, to assess validity of the modeling conditions, a periodic model of the trihydrate structure was created by entering the fractional coordinates of the atoms found by single crystal X-ray diffraction into a unit cell using the Crystal Builder module in Cerius². Hydrogen atoms were then manually added to the water molecules in the model structure. Charge calculation and minimization were then carried out on the periodic structure using the Universal force field module. A comparison of bond distances and angles from the single crystal X-ray diffraction refinement with those found by the trihydrate model in Cerius² are shown in Tables 8 and 9, respectively.

Table 8. Comparison of experimental single crystal X-ray diffraction bond lengths with molecular modeling predicted bond lengths.

Atom 1	Atom 2	Experimental Bond Distance (Å)	Predicted Bond Distance (Å)	% Difference
Ni(1)	C(1)	1.8613	1.868	0.36
N(1)	C(1)	1.1505	1.159	0.74
Fe(1)	N(1)	2.1283	1.958	8.00
Fe(1)	O(1)	2.1965	1.872	14.77

All values were found to be in good agreement with the exception of the Fe^{+2} coordination bond distances. The distances predicted by Cerius² for the Fe^{+2} bonds were slightly smaller than those from the experimental single crystal data. Even with this

discrepancy, the curvature of the sheets remained very close to that found by the single crystal data. An image of the trihydrate model is shown in Figure 6.

Table 9. Comparison of experimental single crystal X-ray diffraction bond angles with molecular modeling predicted bond angles.

Atom 1	Atom 2	Atom 3	Experimental Angle (°)	Predicted Angle (°)	% Difference
O(1)	Fe(1)	N(1)	89.2612	88.8	0.52
Ni(1)	C(1)	N(1)	176.13	177.2	0.61
Fe(1)	N(1)	C(1)	174.33	176.2	1.07

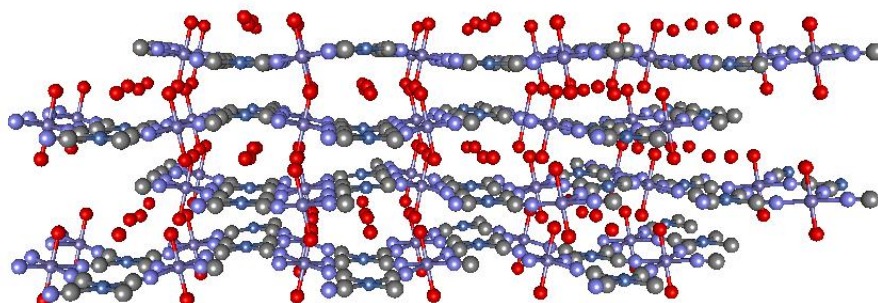


Figure 6. Molecular model of Fe(H₂O)₂Ni(CN)₄·H₂O.

To create the dehydrated model, an extended crystal cell of the trihydrate compound was created with three cell units in the *a* and *b* directions and one unit in the *c* direction to form a 3x3x1 structure which was three sheets thick. The water molecules were removed from the cell, and charge calculation and minimization were carried out. A representation of the resulting model is shown in Figure 7. The model predicts complete flattening of the sheets, as well as the decrease of interlayer spacing upon removal of the water molecules.

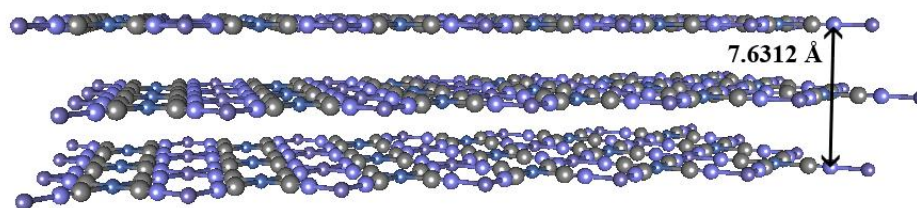


Figure 7. Molecular model of dehydrated FeNi(CN)_4 . The measurement shows the distance between three layers.

3.5 Wide Angle X-Ray Diffraction Results and Discussion

Powder X-ray diffraction data were obtained for compounds with Mn^{2+} , Fe^{2+} , Co^{2+} , Ni^{2+} , Cd^{2+} , and Zn^{2+} metals in the “M” position. The samples for powder diffraction were prepared via the bulk precipitation method. The powder diffraction patterns are shown in Figure 8. All of the compounds except for the Zn^{2+} variety occupied a similar unit cell with minor variations based on differing ionic radii of the “M” metals. Based on the similarities of the powder diffraction data of the Mn^{2+} and Ni^{2+} compounds with that of known Cd^{2+} , Fe^{2+} , and Co^{2+} compounds, along with supporting AFM and SEM evidence of sheet-like structures, it may be assumed that the Mn^{2+} and Ni^{2+} compounds are isostructural to the known compounds (hexahydrates) that were solved by single crystal XRD. The Zn^{2+} variety showed a very different pattern with features characteristic of a partially amorphous substance. This may indicate that the Zn^{2+} variety may possess greater disorder and possibly different morphology than the other compounds.

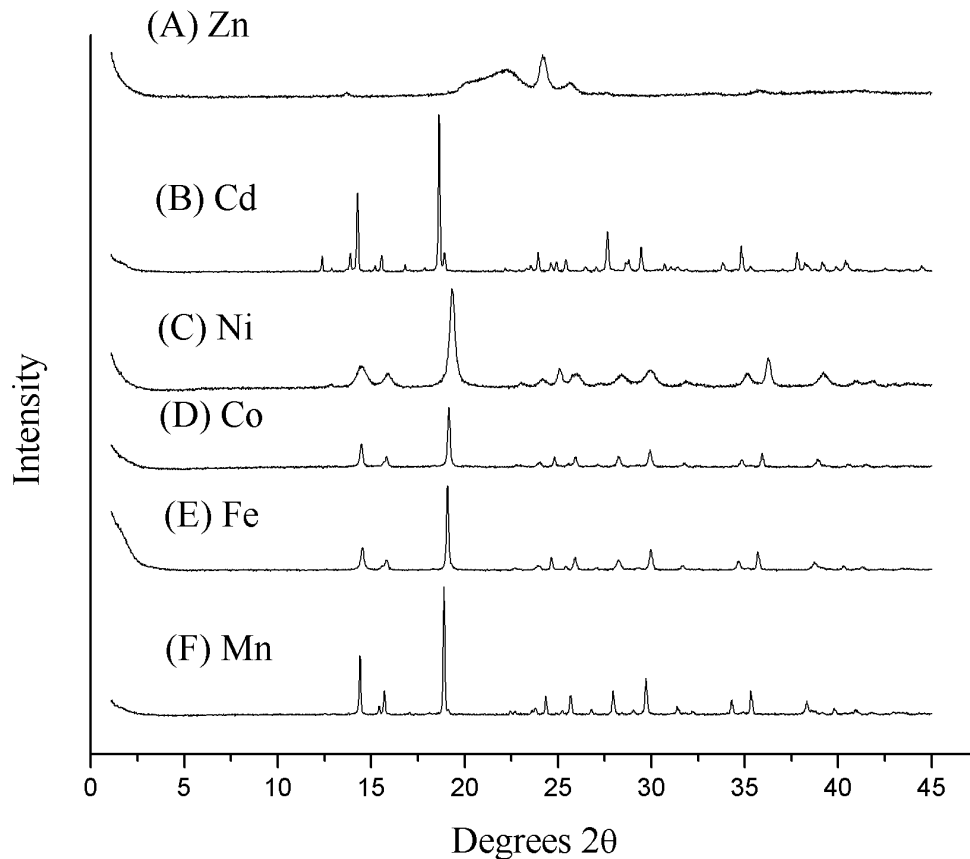


Figure 8. Wide angle XRD patterns for the hydrated compounds. Powder XRD patterns for each of the compounds of the general formula $M(H_2O)_2Ni(CN)_4 \cdot 4H_2O$, where M is (A) Zn^{2+} , (B) Cd^{2+} , (C) Ni^{2+} , (D) Co^{2+} , (E) Fe^{2+} , and (F) Mn^{2+} .

Powder X-ray diffraction was used to monitor the interlayer spacing as intercalation with DDP occurred and as dehydration progressed. A series of dehydrated, trihydrate, hexahydrate, and intercalated powder XRD patterns for $FeNi(CN)_4$ are shown in Figure 9 with the peak corresponding to interlayer distance marked to show progression of expansion. In the fully hydrated structure, Figure 9B, the peak at $14.54^\circ 2\theta$ (6.089 \AA) has Miller indices of 200, corresponding to half the distance of the *a*-axis in the unit cell. This corresponds to the average distance between two adjoining sheets and changes drastically as interlayer molecules are inserted or removed. In the trihydrate,

upon assignment of a new space group, one half distance of the unit cell *c*-axis now correlates to the distance between layers, as can be seen from the single crystal structure. Therefore, in Figure 9C, the peak at $19.82^\circ 2\theta$ (4.476 Å) with Miller indices of 002 corresponds to the average distance between two adjoining sheets. Upon partial dehydration to the trihydrate, the removal of water and partial collapse of the layers on themselves was evident as the d-spacing decreased to 4.476 Å, a decrease of 1.613 Å from the fully hydrated structure.

Since the crystal structure could not be solved for the dehydrated $\text{FeNi}(\text{CN})_4$ structure, molecular modeling was used to approximate the interlayer distance between two adjoining layers. Figure 4 shows a measurement of the distance between three sheets predicted in the model, 7.6312 Å. Dividing this number in half yields a value of 3.8156 Å, which corresponds to the theoretical distance between two layers. Upon comparison of the theoretical value to the powder XRD pattern of the dehydrated structure in Figure 9D, the peak closest to the theoretical value at $23.30^\circ 2\theta$ (3.815 Å) has been marked to correspond with the interlayer d-spacing. Although the predicted value is very close to this peak, this assignment is not absolute as no empirically observed structural data are available for comparison with the powder XRD data for the dehydrated compound.

Upon treatment of the bulk powder with DDP, significant increase in interlayer distance was observed. From molecular modeling using Cerius² by Accelrys®, Inc. using the Compass force field module, the length of a DDP molecule from head to tail was determined to be about 17 Å. The peak at $4.43^\circ 2\theta$ in the intercalated pattern, Figure 9A, has a d-spacing of 19.938 Å, and corresponds to the interlayer distance between two

adjoining sheets. Because the second peak in this pattern at $8.84^\circ 2\theta$ has a d-spacing of 9.992 \AA , or about half the d-spacing of the first peak, it is most likely a 002 reflection from this structure. The d-spacing of the first peak implies that the layer has expanded by exactly one DDP molecule, as the distance of 19 \AA corresponds to the length of one DDP molecule in addition to the DDP \cdots Fe bond length, which would be about 2 \AA , for a total of 19 \AA . The remaining distance of about 1 \AA is most likely the distance between the tail of the DDP molecule and the next layer in the structure. Therefore, the intercalated structure most likely consists of two DDP molecules bonded to the Fe^{2+} in octahedral coordination on either side of the sheet, with the bond taking place on the O atom of the DDP molecule. The DDP tails are oriented perpendicular to the plane of the sheet, pointing directly toward the square hole of the opposing layer. Although it cannot be monitored by powder XRD, as the concentration of DDP increases to great excess, DDP molecules may orient between the layers tail-to-tail, then head-to-head in micelle-like formations, pushing the layers so far apart that the attraction between sheets may become negligible. Sonication provides the shear force necessary to encourage complete separation of individual sheets into a DDP suspension. This process allows individual nanosheets to be separated and deposited on a substrate as DDP is removed.

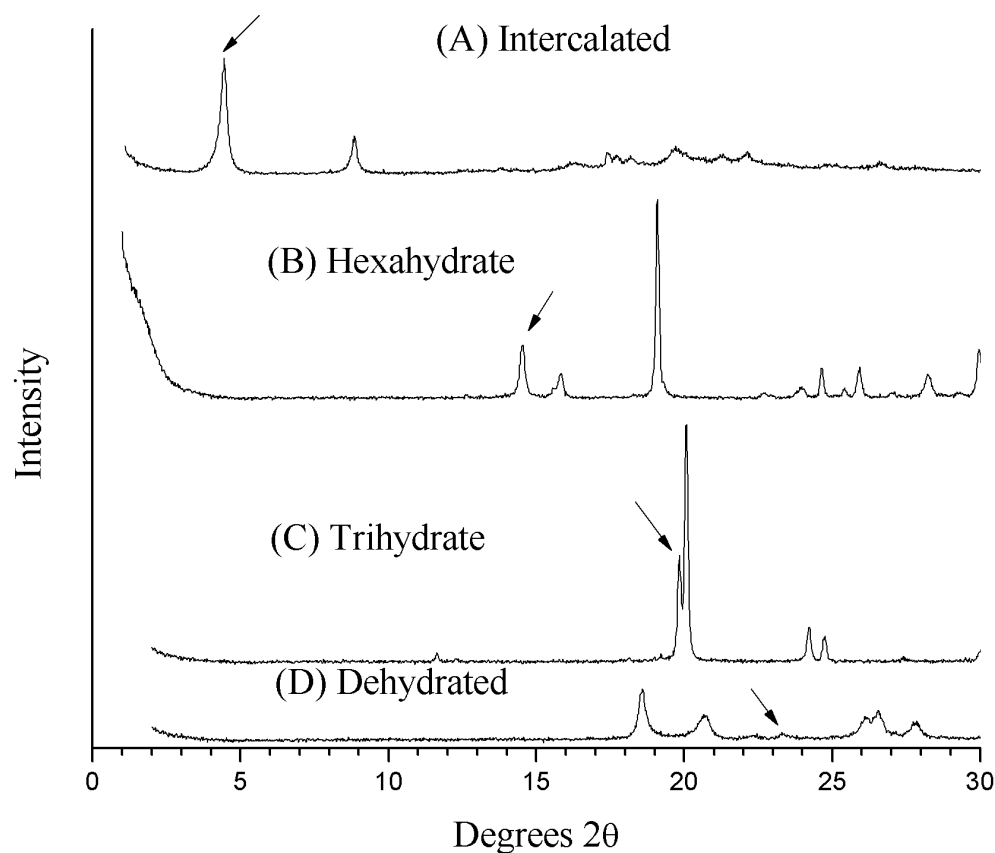


Figure 9. Wide angle XRD patterns showing interlayer expansion. The powder XRD pattern is shown for the (A) intercalated, (B) hexahydrate, (C) trihydrate, and (D) dehydrated $\text{FeNi}(\text{CN})_4$ compounds. The peak corresponding to the distance between two adjoining sheets is labeled with an arrow to monitor expansion of the interlayer d-spacing.

3.6 AFM and SEM Morphological Studies of Individual Nanosheets

Morphological studies were carried out on selected compounds using atomic force microscopy (AFM) and scanning electron microscopy (SEM). All samples were heated to dehydration temperatures before imaging. Images obtained via SEM and AFM analysis revealed single nanosheets ranging in width from about 200 nm to 1.2 μm . A typical image of single $\text{MnNi}(\text{CN})_4$ nanosheets is shown in Figure 10A. A multilayered

CoNi(CN)_4 structure can be seen next to a single sheet of about 200 nm in Figures 10C and 10D, respectively. Although a large number of single nanosheets were located, a small portion of unseparated multilayer structures were also found. The thickness of single sheets was found to be about 0.2 nm by AFM analysis. Figure 11A shows a cross-sectional analysis of a single sheet of MnNi(CN)_4 , while Figure 11B presents a 3-D projection of the same image. This thickness corresponds to a single molecular layer, as can be seen from single crystal X-ray diffraction data from the parent 3-D structure.

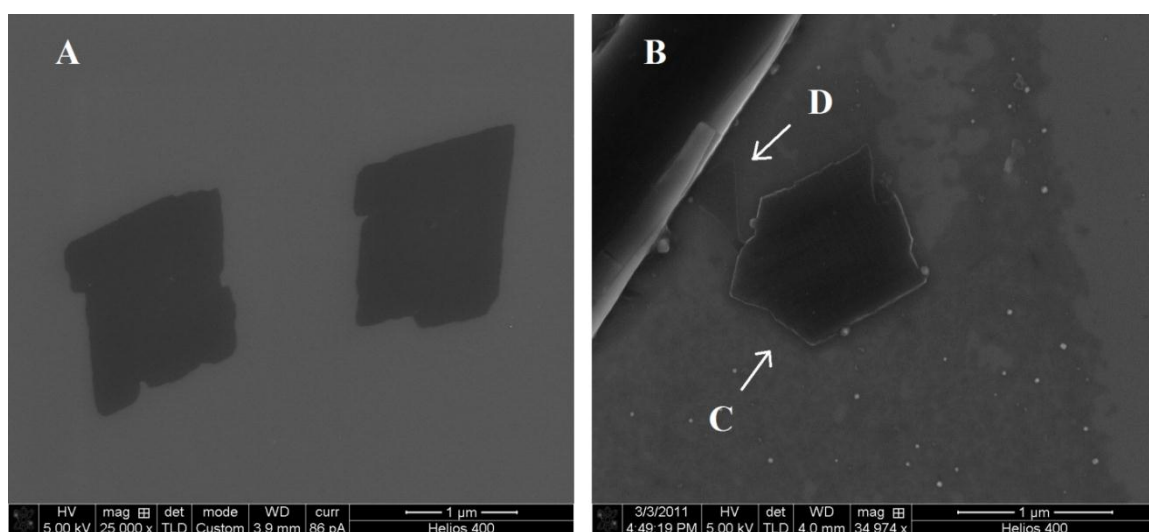


Figure 10. SEM images of nanosheets. An SEM image of (A) two similar single MnNi(CN)_4 nanosheets is shown along with an image of (B) CoNi(CN)_4 nanoparticles. The (C) large sheet in the middle is most likely a multilayer structure, while the (D) smaller triangular piece next to it is most likely a single molecular layer.

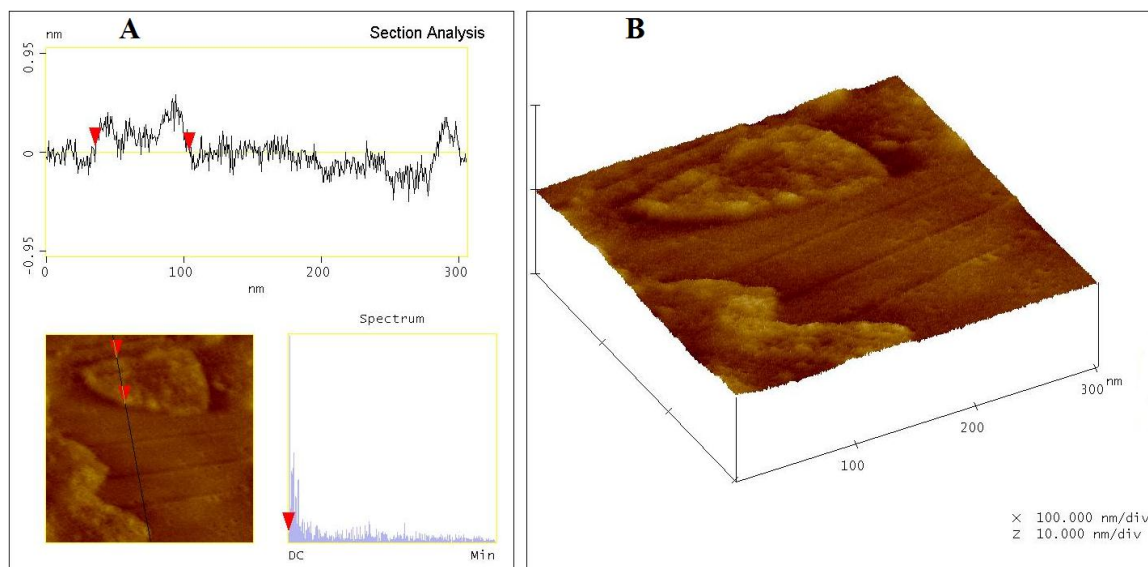


Figure 11. AFM analysis of MnNi(CN)_4 nanosheet. A (A) cross-sectional analysis of an AFM image is shown for a single nanosheet of MnNi(CN)_4 along with a (B) 3-D projection of the same nanosheet. The average height of the nanosheet is about 0.2 nm, and the width at its widest point is about 200 nm.

CHAPTER 4

CONCLUSION

Various $M(H_2O)_2Ni(CN)_4$ compounds were characterized. The crystal structures of $Fe(H_2O)_2Ni(CN)_4 \cdot 4H_2O$, $Fe(H_2O)_2Ni(CN)_4 \cdot H_2O$, and $Cd(H_2O)_2Ni(CN)_4 \cdot 4H_2O$ were found to consist of two-dimensional sheets bound together by hydrogen-bonded and octahedrally coordinated water molecules. The $Fe(H_2O)_2Ni(CN)_4 \cdot H_2O$ structure is the product of loss of the water molecules only held in the structure by hydrogen bonding, and this finding was also consistent with TGA data. The trihydrate structure also revealed that the sheets flatten as the water molecules are removed. Although no crystal structure was solved for the completely dehydrated structure, molecular modeling reinforced the idea that the sheets completely flatten upon removal of water. A method was successfully developed to exfoliate individual nanosheets from the parent multilayer structures using DDP. The expansion of the layers was monitored by powder X-ray diffraction and found to be consistent with intercalation of DDP into the inner layer space. The separation of individual nanosheets was confirmed by AFM and SEM imaging.

Currently, work is being conducted to obtain magnetic and electrical measurements on the exfoliated nanosheets for possible applications in nanoscale electronics. Future studies may be performed to enhance the quality of nanosheets

produced by this method. Variation of sonication conditions, heating times and temperature, substrate, and concentration may allow for better control of the end product. Control of nanosheet size and uniform dispersion on a substrate are goals for future study. The extent of exfoliation may also be increased by varying these types of factors.

REFERENCES

1. Novoselov, K. S.; Geim, A. K.; Morozov, S. V.; Jiang, D.; Zhang, Y.; Dubonos, S. V.; Grigorieva, I. V.; Firsov, A. A. Electric Field Effect in Atomically Thin Carbon Films. *Science* **2004**, 306 (5696), 666-669.
2. Novoselov, K. S.; Jiang, D.; Schedin, F.; Booth, T. J.; Khotkevich, V. V.; Morozov, S. V.; Geim, A. K. Two-dimensional atomic crystals. *Proc Nat Acad Sci USA* **2005**, 102 (30), 10451-10453.
3. Rao, C.N.R.; Sood, A.K.; Subrahmanyam, K.S.; Govindaraj, A. Graphene: The New Two-Dimensional Nanomaterial. *Angew. Chem. Int. Ed.* **2009**, 48, 7752-7777.
4. Avouris, P. Graphene: Electronic and Photonic Properties and Devices. *Nano Lett.* **2010**, 10, 4285-4294.
5. Stoller, M.D.; Park, S.; Zhu, Y.; An, J.; Ruoff, R.S. Graphene-Based Ultracapacitors. *Nano Lett.* **2008**, 8, 3498-3502.
6. Castro Neto, A.H.; Guinea, F.; Peres, N.M.R.; Novoselov, K.S.; Geim, A.K. The electronic properties of graphene. *Rev. Mod. Phys.* **2009**, 81, 109.
7. Leng, Yonghua; Zhang, Yaohua; Liu, Tong; Suzuki, Masaaki; Li, Xingguo. Synthesis of single crystalline triangular and hexagonal Ni nanosheets with enhanced magnetic properties. *Nanotechnology* **2006**, 17(6), 1797-1800.
8. Osada, Minoru; Sasaki, Takayoshi. Exfoliated oxide nanosheets: new solution to nanoelectronics. *J. Mater. Chem.* **2009**, 19, 2503-2511.
9. Schniepp, H.C. *et al.* Functionalized Single Graphene Sheets Derived from Splitting Graphite Oxide. *J. Phys. Chem. B* **2006**, 110, 8535-8539.
10. Ma, R.; Liu, Z.; Li, L.; Iyi, N.; Sasaki, T. Exfoliating layered double hydroxides in formamide: a method to obtain positively charged nanosheets. *J. Mater. Chem.* **2006**, 16, 3809-3813.
11. Fukuda, K. *et al.* Exfoliated Nanosheet Crystallite of Cesium Tungstate with 2D Pyrochlore Structure: Synthesis, Characterization, and Photochromic Properties. *ACS Nano* **2008**, 2, 1689-1695.

12. Wilde, Richard E.; Ghosh, Surendra Nath; Marshall, Billy J. Prussian blues. *Inorg. Chem.* **1970**, 9(11), 2512-2516.
13. Harper, S.D. Preparation of lactone polymers using double metal cyanide catalysts. U.S. Patent 5,032,671, July 16, 1991.
14. Grosch, Georg Heinrich; Larbig, Harald; Lorenz, Reinhard; Junge, Dieter; Kammel, Ulrich. Manufacture of supported double metal cyanide catalysts and their use for producing polyether alcohols. U.S. Patent 6,362,126, March 26, 2002.
15. Iwamoto, Toschitake. Past, present and future of the clathrate inclusion compounds built of cyanometallate hosts. *J. Incl. Phenom. Macro.* **1996**, 24(1-2), 61-132.
16. Iwamoto, T.; Nakano, T.; Morita, M.; Miyoshi, T.; Miyamoto, T.; Sasaki, Y. The metal ammine cyanide aromatics clathrates. V. The Hofmann-type clathrate: $M(NH_3)_2M'(CN)_4 \cdot 2G$. *Inorg. Chim. Acta*, **1968**, 2(3), 313-316.
17. Mathey, Y.; Mazieres, C. Phases of nickel(II) cyanide hydrates. *Can. J. Chem.* **1974**, 52(21), 3637-3644.
18. Niu, Tianyan; Crisci, Gerardo; Lu, Jian; Jacobson, Allan J. Diaquacobalt Tetracyanonickelate Hexahydrate. *Acta Cryst.* **1998**, 54, 565-567.
19. Ham, William K.; Weakley, Timothy J. R.; Page, Catherine J. Synthesis and Crystal Structure of $Cd(H_2O)_2Ni(CN)_4 \cdot 4H_2O$. *J. Solid State Chem.* **1993**, 107(1), 101-107.
20. Higgins, Craig. The electronic structure properties of monolayer transition metal cyanides. M.S. Thesis, Texas State University–San Marcos, San Marcos, TX, 2010.
21. Culp, Jeffrey T.; Park, Ju-Hyun; Meisel, Mark W.; Talham, Daniel R. Interface directed assembly of cyanide-bridged Fe–Co and Fe–Mn square grid networks. *Polyhedron* **2003**, 22, 3059-3064.
22. Culp, J. T.; Park, J.-H.; Stratakis, D.; Meisel, M. W.; Talham, D.R. Supramolecular Assembly at Interfaces: Formation of an Extended Two-Dimensional Coordinate Covalent Square Grid Network at the Air–Water Interface. *J. Am. Chem. Soc.* **2002**, 124, 10083-10090.
23. Culp, J.T.; Park, J.-H.; Meisel, M. W.; Talham, D.R. Monolayer, Bilayer, Multilayers: Evolving Magnetic Behavior in Langmuir–Blodgett Films Containing a Two-Dimensional Iron–Nickel Cyanide Square Grid Network. *Inorg. Chem.* **2003**, 42, 2842-2848.
24. Beall, G.W.; Goss, M. Self-assembly of organic molecules on montmorillonite. *Applied Clay Science* **2004**, 27, 179-186.

25. Coleman, J.N. *et al.* Two-Dimensional Nanosheets Produced by Liquid Exfoliation of Layered Materials. *Science* **2011**, 331, 568-571.
26. Hernandez, Y. *et al.* High-yield production of graphene by liquid-phase exfoliation of graphite. *Nat Nano* **2008**, 3, 563-568.
27. CrystalClear: Rigaku Corporation, 1999. CrystalClear Software User's Guide, Molecular Structure Corporation, © 2000. J.W. Pflugrath (1999) *Acta Cryst.* D55, 1718-1725.
28. PATY: Beurskens, P.T.; Admiraal, G.; Behm, H.; Beurskens, G.; Smits, J.M.M.; Smykalla, C. (1991). *Z. f. Kristallogr. Suppl.* 4, p.99.
29. Carruthers, J.R.; Watkin, D.J. *Acta Cryst.* **1979**, A35, 698-699.
30. Cromer, D. T.; Waber, J. T. "International Tables for X-ray Crystallography", Vol. IV, The Kynoch Press, Birmingham, England, Table 2.2 A (1974).
31. Ibers, J. A.; Hamilton, W. C. *Acta Cryst.* **1964**, 17, 781.
32. Creagh, D. C.; McAuley, W.J. "International Tables for Crystallography", Vol C, (A.J.C. Wilson, ed.), Kluwer Academic Publishers, Boston, Table 4.2.6.8, pages 219-222 (1992).
33. Creagh, D. C.; Hubbell, J.H. "International Tables for Crystallography", Vol C, (A.J.C. Wilson, ed.), Kluwer Academic Publishers, Boston, Table 4.2.4.3, pages 200-206 (1992).
34. CrystalStructure 4.0: Crystal Structure Analysis Package, Rigaku and Rigaku Americas (2000-2010). 9009 New Trails Dr., The Woodlands TX 77381 USA.
35. CRYSTALS Issue 11: Carruthers, J.R.; Rollett, J.S.; Betteridge, P.W.; Kinna, D.; Pearce, L.; Larsen, A.; Gabe, E. Chemical Crystallography Laboratory, Oxford, UK. (1999)

VITA

Tyler Lee Nash was born in Austin, Texas on March 17, 1987, the son of Michael Dean Nash and Patti Renee Nash, and the sibling of Brian Dean Nash. After completing his work at Nash Homeschool Academy, Dripping Springs, Texas and Austin Community College, Austin, Texas, in 2004, he entered the University of Texas at Dallas. In fall of 2006, he transferred to Texas State University-San Marcos, San Marcos, Texas where he received the degree of Bachelor of Science with a major in Chemistry and a minor in Geology in May 2011. He entered into the graduate program at Texas State under the Early Entry M.S. program in fall of 2010 with a major in Chemistry. In March 2011, he married his wife, Dr. Yelena Vecherkina Nash. He hopes to enter the upcoming Materials Science, Engineering, and Commercialization program at Texas State as a Ph. D candidate in spring of 2012. His favorite pastimes include mountain biking, camping, hiking, fishing, off road vehicles, cooking, and gardening with his wife.

Permanent Address: 501 Mussey Road

Dripping Springs, TX 78620



This thesis was typed by Tyler Lee Nash.